CHAPTER III
RESULTS AND DISCUSSION

In this chapter, the measurements in and the descriptions of binary systems of pure polymer and surfactant in aqueous solution (HPC/water and HTAB/water) and the ternary systems (HPC/HTAB/water) of both dilute and concentrated solutions will be described.

3.1 Dilute Solution : Determination of Maximum Binding Point

3.1.1 Binary System (HPC/Water)

3.1.1.1 Viscosity Viscosity measurements on dilute aqueous solutions of hydroxypropylcellulose, HPC, were performed using the Ubbelohde capillary viscometer size 50. Figure 3.1 shows reduced viscosity, η_{sp}/C_{HPC} and inherent viscosity, ln η_r/ C_{HPC}, for HPC solutions versus polymer concentration, C_{HPC} at 30°C . The data points suggest linear dependence of reduced viscosity and inherent viscosity with polymer concentration. Straight lines can be drawn through η_{sp}/C_{HPC} versus C_{HPC} and ln η_r/C_{HPC} versus C_{HPC} according to the Huggins equation (Equation 2.1) and the Kraemer equation (Equation 2.2) respectively. Intrinsic viscosity was determined by intercept of these straight lines and the results are shown in Table 3.1. From slope of the Huggins plot, Huggins constant was also obtained. The value represents the interaction between solvent and HPC. In this case, k_H is about 0.9 which shows that water is a poor solvent for this system and k_K is about 0.003. Kraemer plot gives Kraemer constant, k_K and the value is about 0.003.

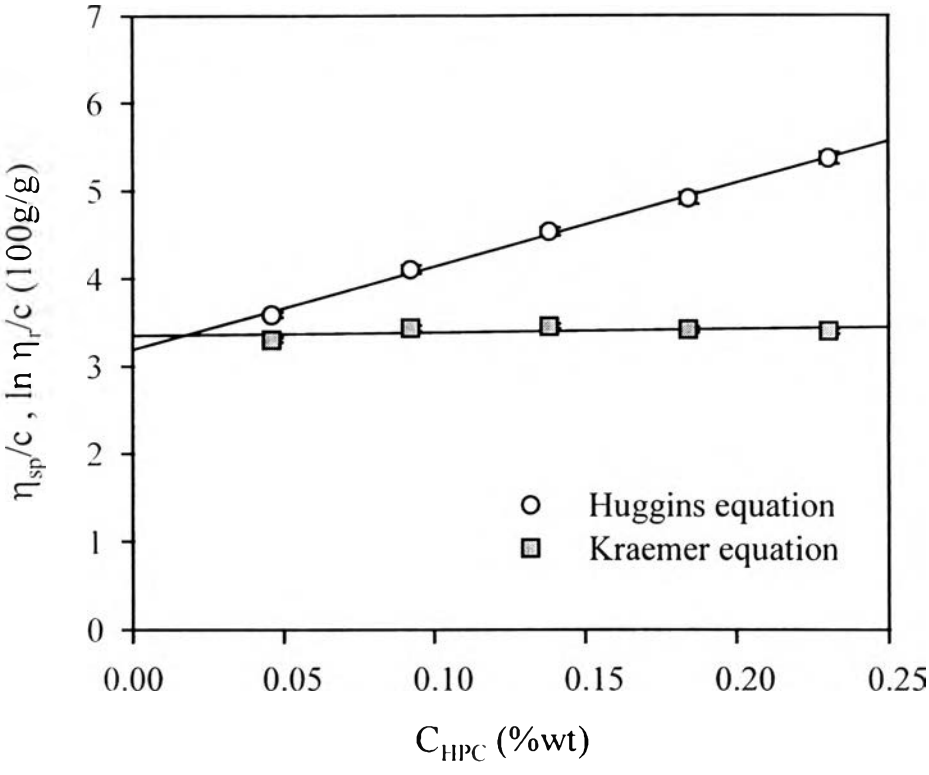

Figure 3.1 Reduced viscosity and inherent viscosity for hydroxypropyl-cellulose in water as a function of polymer concentration at 30°C: (O) reduce viscosity, (▣) inherent viscosity.

The overlap concentration C^*_{HPC} is the concentration at which polymer chains begin to overlap each other; C^*_{HPC} can be defined by

$$C^* = 1/[\eta] \tag{3.1}$$

so C^*_{HPC} of this system is equal to 0.31%wt. Figure 3.2 shows data on the concentration dependence of the dynamic viscosity, η, extending to semidilute concentration region. It can be observed that η increases monotonically with polymer concentration. At low C_{HPC}, η has a linear dependence with polymer concentration until it reaches the polymer concentration of 0.3 %wt where the curve starts to bend upward. Above 0.3%wt, the solutions are semidilute.

Intermolecular and entanglement interactions occur. The value of C^*_{HPC} = 0.3%wt was obtained from the bending of η versus C_{HPC} of Figure 3.2 which is consistent with the value from the intrinsic viscosity obtained from the intercept of Figure 3.1.

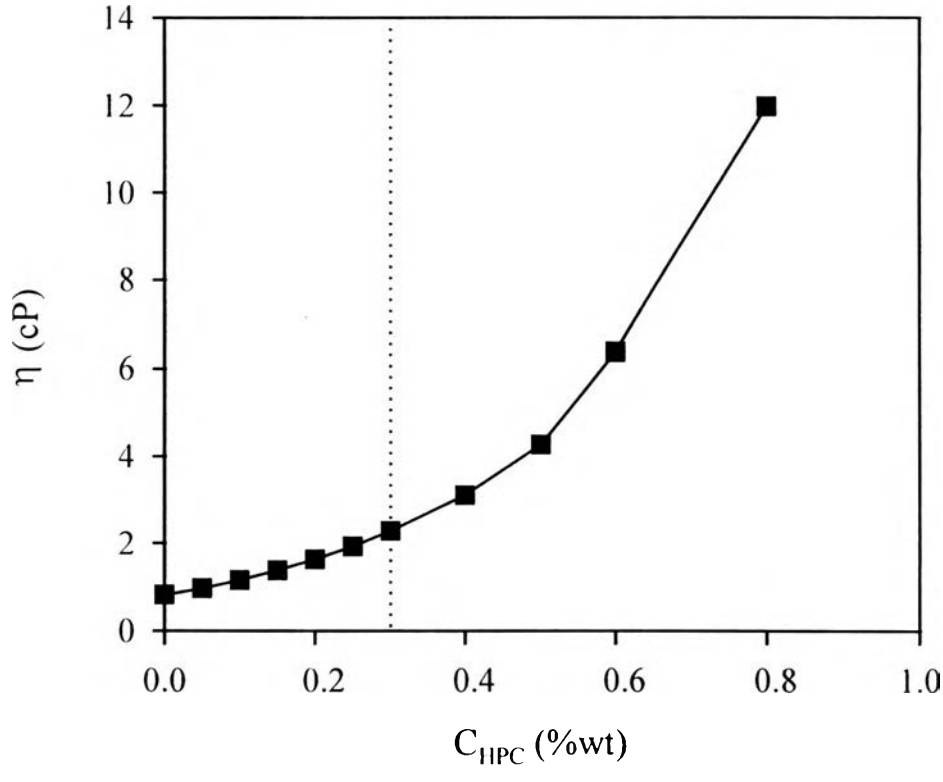

Figure 3.2 Dynamic viscosity for hydroxypropylcellulose as a function of polymer concentration at 30°C.

3.1.1.2 Dynamic Light Scattering Dynamic light scattering measurement can be applied to study properties of dilute polymer solutions. The translational motions of the polymer coils can be determined when $qR_g << 1$ and the internal motions of large single coils can be measured when $qR_g > 1$. Figure 3.3 shows the apparent diffusion coefficient, D_{app}, for HPC solution of fixing C_{HPC} at 0.1%wt as a function of scattering wave vector square, q^2, at scattering angle from 75° to 120° at 30°C. D_{app} has a linear dependence on q^2 according to Equation 3.2,

$$D_{app} = D_{CM}(1 + f_c q^2 R_g^2) \quad (3.2)$$

where D_{CM} is center of mass diffusion coefficient, f_c is a dimensionless number which depends on chain structure, polydispersity and solvent quality [Burchard, 1993]. The linear regression line can be drawn through all data points. The positive slope represents a mixture of the translational and internal motions. The center of mass diffusion coefficient can be obtained from the intercept. The similar graphs for other polymer concentrations are shown in Appendix.

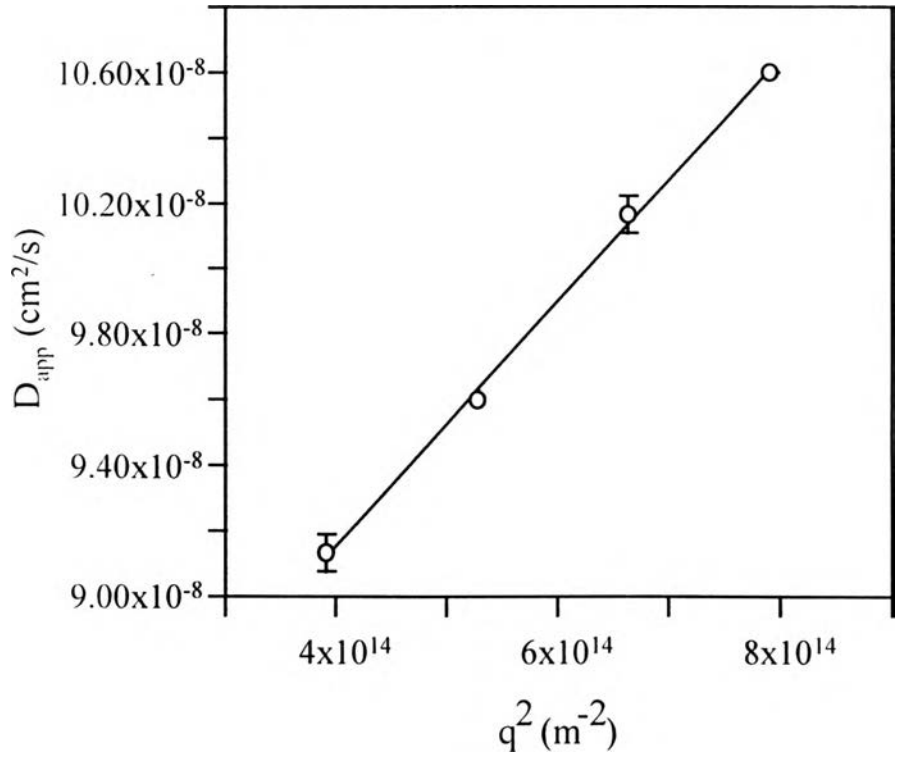

Figure 3.3 Apparent diffusion coefficient for HPC in water at fixing C_{HPC} of 0.10%wt as a function of scattering wave vector square at 30°C.

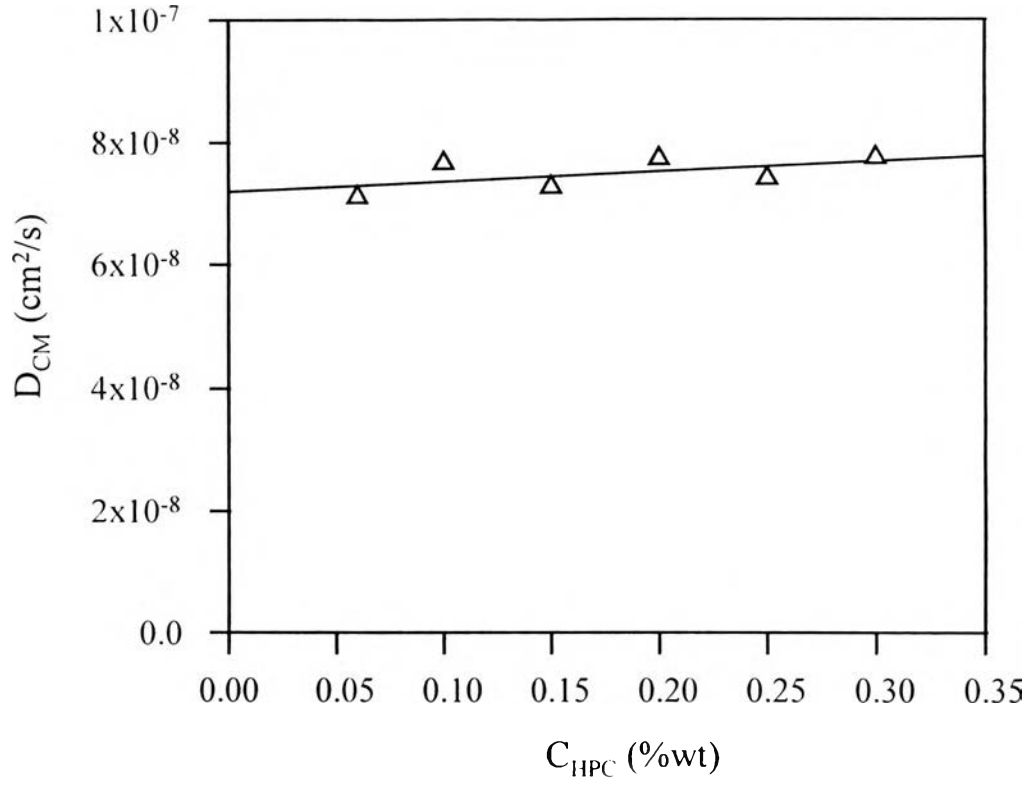

Figure 3.4 Center of mass diffusion coefficient for HPC in water as a function of polymer concentration at 30°C.

Figure 3.4 shows the concentration dependence of the center of mass diffusion coefficient as a function of polymer concentration at 30°C. All data points follow a linear dependence which can be written as the following equation:

$$D_{CM} = D_o(1+k_D C), \tag{3.3}$$

where $k_D = 2A_2M - k_f - V_2$, A_2 is the second virial coefficient, M is molecular weight, k_f is the concentration dependence of the frictional coefficient and V_2 is the partial specific volume. Since water is a poor solvent for this polymer, the second virial coefficient, A_2, is small and therefore D_{CM} slightly increases with increasing polymer concentration [Brown, 1993]. From the intercept of this

line, the diffusion coefficient of infinite dilution, D_0, was obtained and then converted to the hydrodynamic radius, R_h, by using the Stoke-Einstein equation (Equations 2.25 and 2.26). R_h of HPC is 37.4nm.

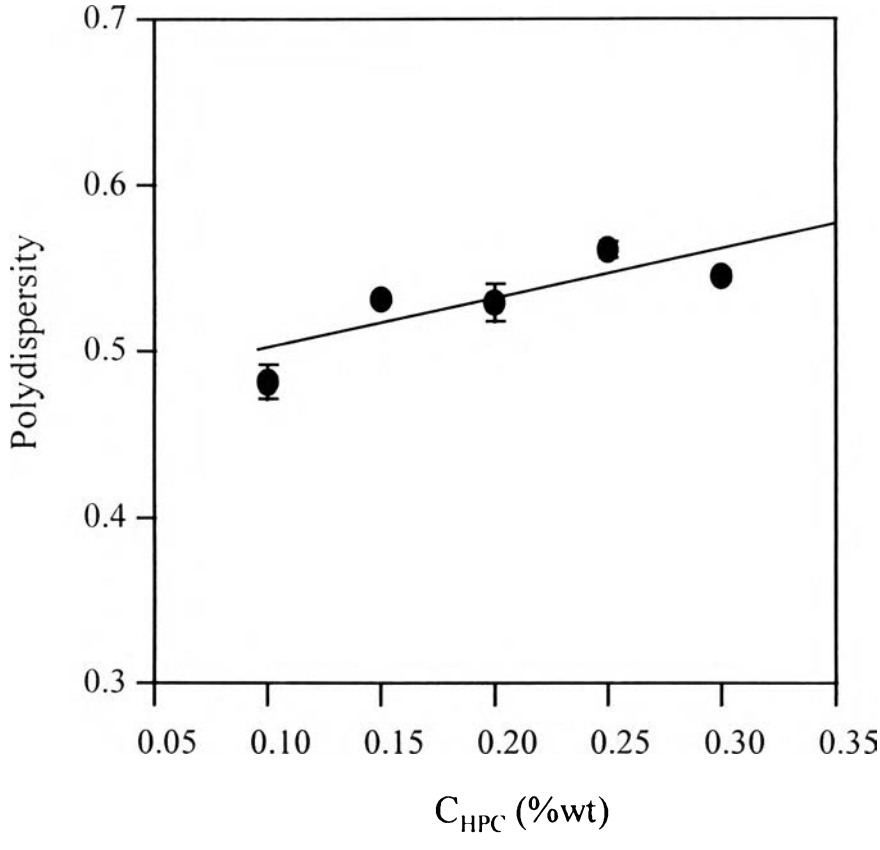

Figure 3.5 Polydispersity of relaxation time for hydroxypropylcellulose solutions at 90° as a function of polymer concentration at 30°C.

Figure 3.5 shows polydispersity of relaxation time for HPC solution which is equal to $(\langle\Gamma'\rangle/\langle\Gamma\rangle)^2$ versus polymer concentration at the scattering wave vector of 90°. $\langle\Gamma'\rangle$ is a standard deviation of characteristic decay time and $\langle\Gamma\rangle$ is a mean of characteristic decay time. The polydispersity slightly increases with polymer concentration. The range of polydispersity covers from 0.47 to 0.57.

3.1.1.3 Static Light Scattering Zimm plot analysis was applied to determine the weight-average molecular weight and the radius of gyration, R_g, of HPC. Figure 3.6 shows Zimm plot for HPC samples in water at 30°C. The differential index increment (dn/dc) for HPC in water was determined to be 0.137 ml/g (Figure 2.3). From Equations 2.20 and 2.21, the molecular weight was obtained from the inverse of the intercept of lines $C_{HPC} = 0$ and $\theta = 0$ in the Zimm plot. The slope of the zero-concentration line as a function of angle provides a measure of R_g.

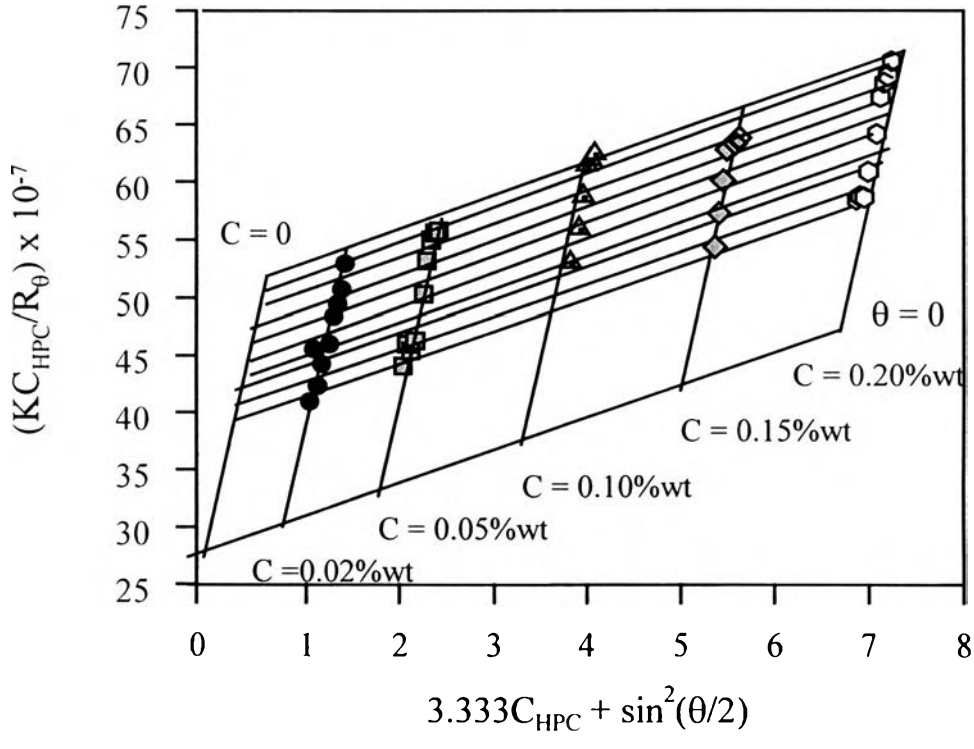

Figure 3.6 Zimm plot for light-scattering intensities of hydroxypropylcellulose solutions at 30°C.

The experimental results of molecular weight, intrinsic viscosity, overlap concentration, diffusion coefficient, hydrodynamic radius and radius of gyration of HPC are compared with values from Yang and Jamieson results

(1988) for the same commercial product and specifications and are summarized in Table 3.1.

Table 3.1 Dynamic properties of HPC in aqueous solutions

Results	MW by Zimm analysis	$[\eta]$ (100g/g)	k_H	k_K	C* (%wt)	D_o (cm^2/s)	R_H	R_g (nm)
Present work	376,935	3.22	0.9	0.003	0.31	$5.6x10^8$	37.37	58.8
Yang & Jamieson	450,000	3.25	-	-	-	$7.8x10^8$	31.40	62.0

The ratio of R_g/R_h for HPC is 1.57. It is fairly close to theoretical value 1.50 for monodisperse random coil at theta conditions [Burchard, 1993]. This interpretation is consistent with the result from k_H.

3.1.2 Binary System (HTAB/Water)

There are several methods to determine the cmc value. In the present system, it is suitable to use both surface tension and conductivity measurements at 28±1°C. Figures 3.7 and 3.8 show surface tension and conductivity versus surfactant concentration of HTAB solutions.

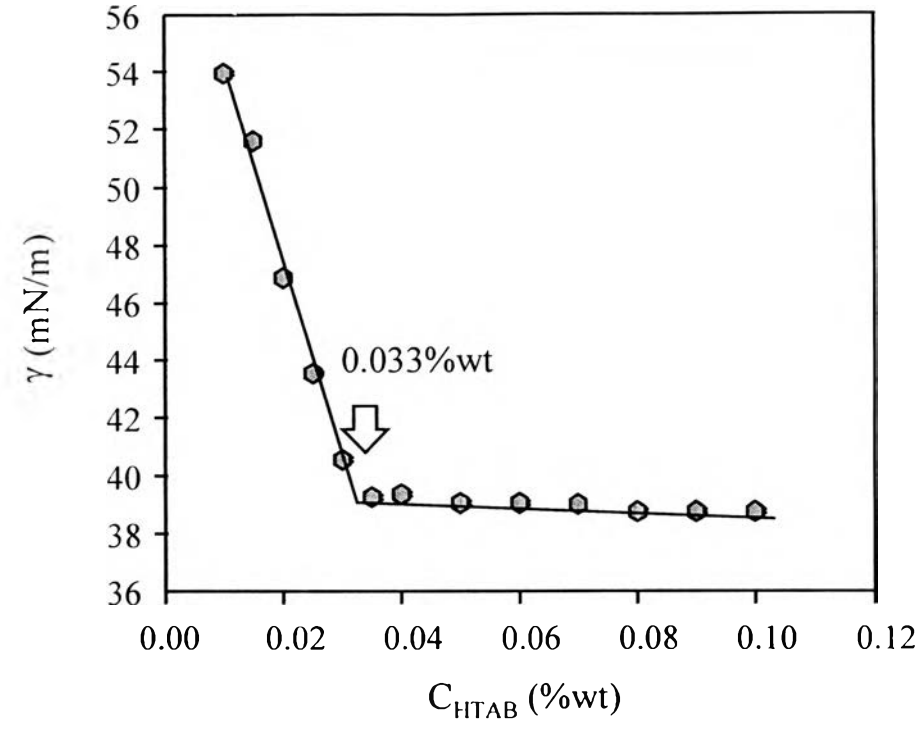

Figure 3.7 Surface tension for HTAB solution versus surfactant concentration at 28±1°C.

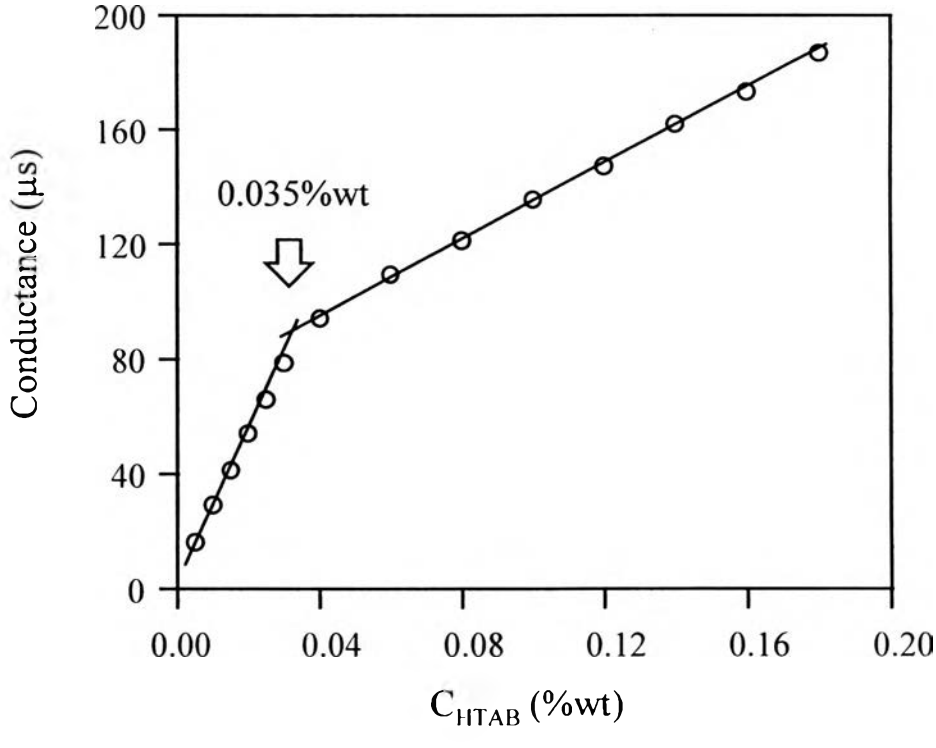

Figure 3.8 Conductance for HTAB solution versus surfactant concentration at 28±1°C.

The point at which slopes abruptly change in both graphs represents the cmc value which is about 0.033%wt (0.91mM) from surface tension or 0.035%wt (0.96mM) from the conductivity measurement. These results are well in agreement with the work of Czemiawski (1966) where they found the cmc of HTAB at 25°C by surface tension to be equal to 0.92mM.

3.1.3 Ternary System (HPC/HTAB/Water)

Figure 3.9 shows critical aggregation concentration, cac, on HPC/HTAB/water system which was determined at a fixed HPC concentration of 0.04 %wt as a function of HTAB concentration. A measurement of surface tension is a convenient method that can be used to find cac. From the plot of surface tension at 28±1°C, as expressed in mN/m, cac is about 0.018%wt of HTAB concentration. This shows that polymer and surfactant molecules start to form complex at a lower surfactant concentration than the normal cmc. The similar result was studied on PVP/SDS system at various PVP concentrations by Jones [1967]. She found the cac is lower than cmc for nonionic polymer and anionic surfactant.

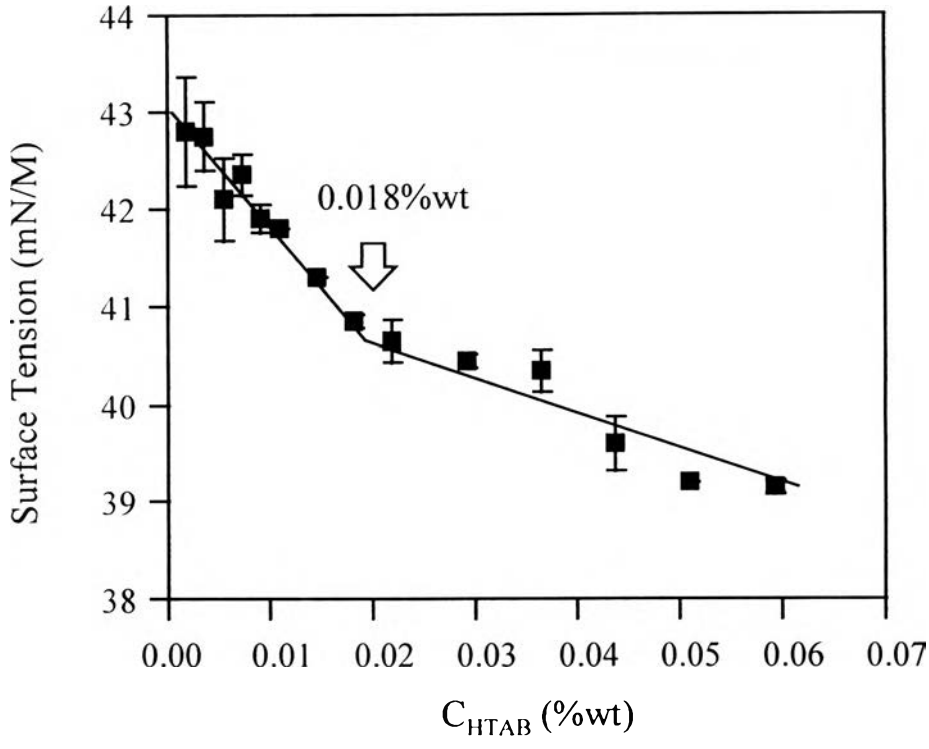

Figure 3.9 Surface tension for complex system at the fixed C_{HPC} of 0.04%wt as a function of surfactant concentration at 28±1°C.

3.1.3.1 Effect of Surfactant Concentration Viscosity measurement was carried out to study the effect of surfactant concentration. Specific viscosity is used here instead of the reduced viscosity since the concentration of the complex is unknown. Specific viscosities were determined at a fixed C_{HPC} of 0.06%wt as a function of surfactant concentration. The result, shown in Figure 3.10, is demonstrated by dividing C_{HTAB} into 4 regions. (I) At C_{HTAB}<0.01%wt, before reaching cac, η_{sp} is constant and independent of the total surfactant concentration. (II) When C_{HTAB} is higher than cac, η_{sp} decreases and shows a shallow minimum at C_{HTAB} = 0.03%wt which is the cmc of pure surfactant system. (III) In middle range of surfactant concentration, η_{sp} becomes very sensitive to the amount of HTAB present. The curve increases abruptly until it reaches the maximum binding point at C_{HTAB} = 0.08%wt. (IV)

At higher surfactant concentration, η_{sp} decreases again. These results can be explained by physical models in Figure 3.11.

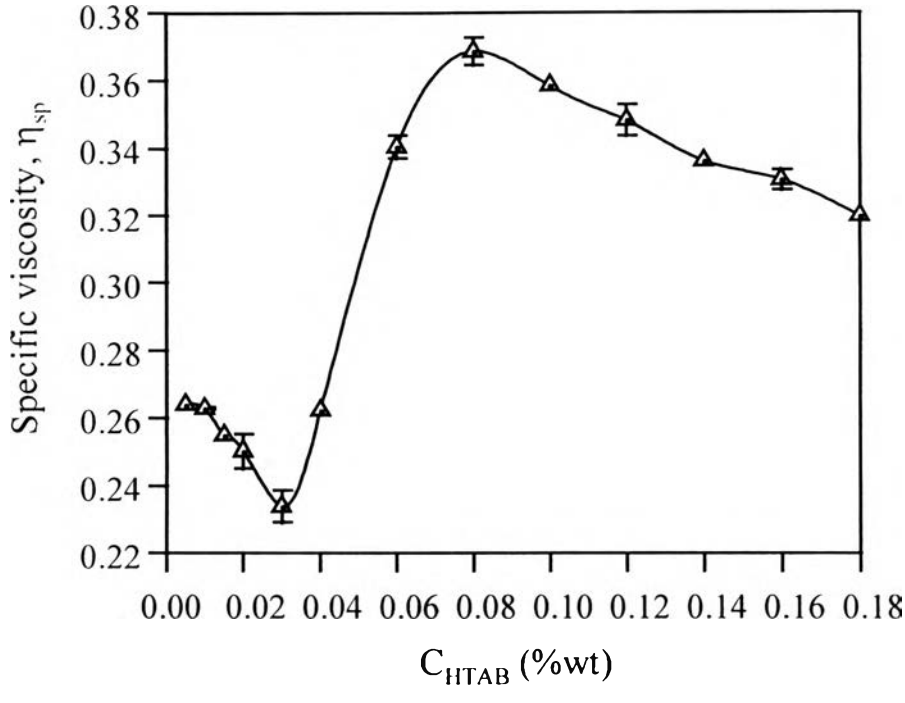

Figure 3.10 Specific viscosity for complex solution at the fixed C_{HPC} of 0.06%wt as a function of surfactant concentration at 30°C.

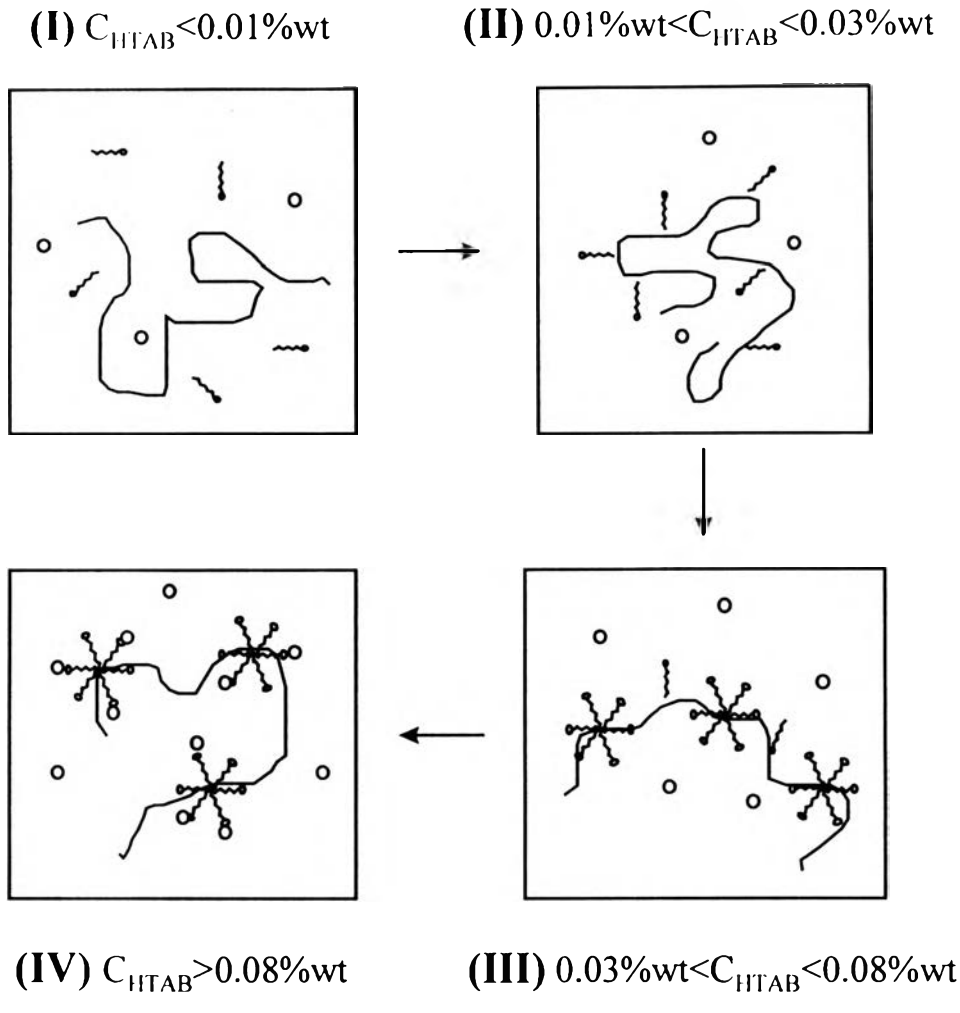

Figure 3.11 Schematic representation of the interaction between HPC and HTAB in ternary system.

Region I : In solution of HPC containing low concentrations of HTAB such that the cac is not exceeded, specific viscosity is constant. HPC is still a neutral polymer and most of the surfactants exist freely in the form of monomers.

Region II : When HTAB concentration exceeds the cac, complex formation occurs, specific viscosity slightly decreases due to the hydrophobic interaction of surfactant tails trying to form micelles.

Region III : At cmc, micelles start to form and bind onto the HPC chains, repulsive interactions take place. Consequently, the HPC chains expand until it reaches the maximum binding point. This point indicates the most extended conformation of the HPC chains. Further binding is inhibited by electrostatic repulsion between micelles, so no more binding of HTAB on HPC chains occurs when increasing the HTAB concentration.

Region IV : The decrease in specific viscosity when HTAB concentration is above maximum binding is owning to the effect of counterions (Br^-) or the screening effect which can reduce the repulsive interactions between micelles bound onto the HPC chains.

A similar results were obtained for EHEC-SDS and HPMC-SDS systems as reported by Nilsson [1995].

3.1.3.2 Effect of Polymer Concentration on the Maximum Binding Point In Figure 3.12, the results from viscosity measurements depicts the effect of polymer concentration on the maximum binding point. The experiments were performed for selected values of polymer concentrations in the range 0.02 to 0.10%wt and for surfactant content varying from 0 to 0.18%wt. The results have been obtained at 30°C. Increasing polymer concentration will shift the maximum binding point to a higher surfactant concentration

These results show that the greater number polymer chains in solution. the more content of surfactants are needed or required to bind with the polymer chains to reach the saturation state. The maximum binding points of each curve are tabulated in Table 3.2.

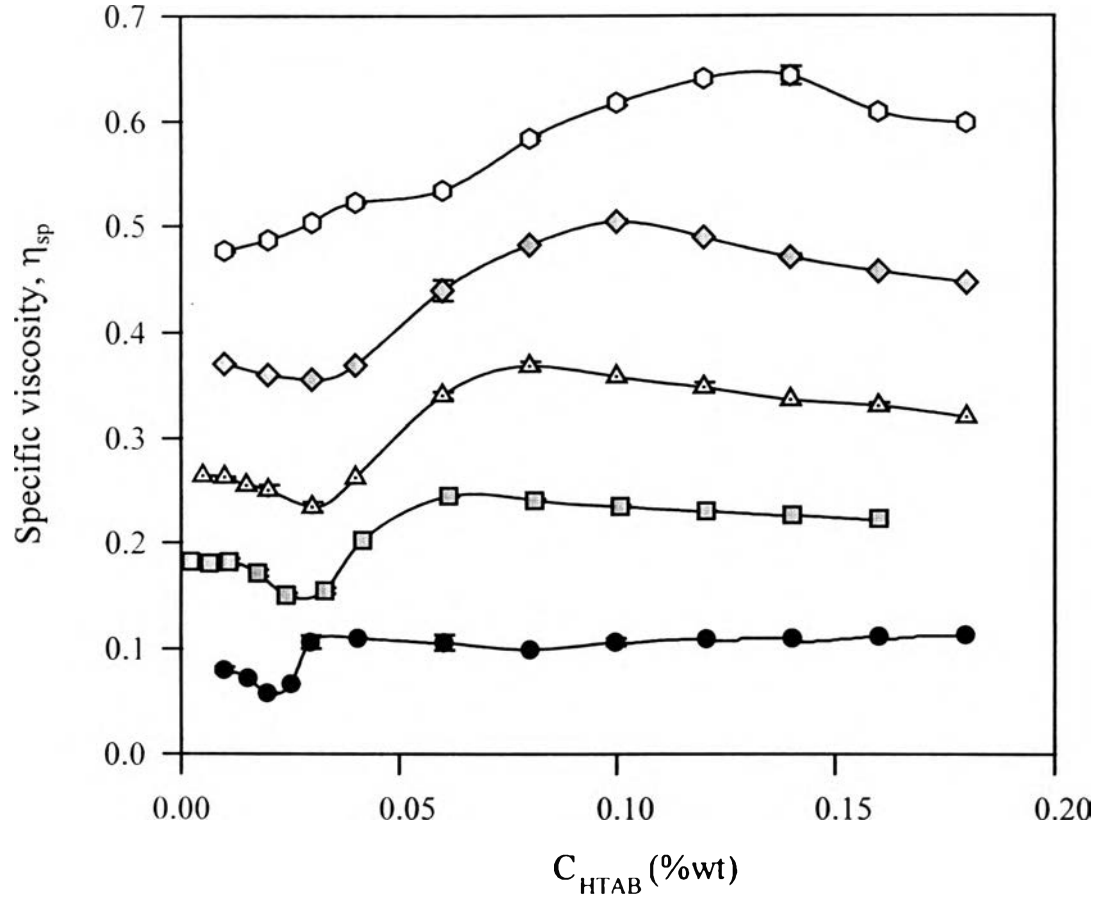

Figure 3.12 Specific viscosity of complex system at different polymer concentrations as a function of surfactant concentration at 30°C: (●) C_{HPC} = 0.02%wt, (▣) C_{HPC} = 0.04%wt, (△) C_{HPC} = 0.06%wt, (◇) C_{HPC} = 0.08%wt and (⬡) C_{HPC} = 0.10%wt.

Dynamic light scattering measurement of complex system can also be used to find maximum binding point. The analysis method was the same as in polymer system. Figure 3.13 shows D_{app} for complex solution of fixing C_{HPC} at 0.10%wt as a function of q^2 at scattering angles from 75° to 120° at 30°C. D_{app} also has a linear dependence on q^2 according to Equation 3.2. The positive slope can be observed due to a mixture translational and internal motions. Other graphs at other polymer concentrations are shown in Appendix.

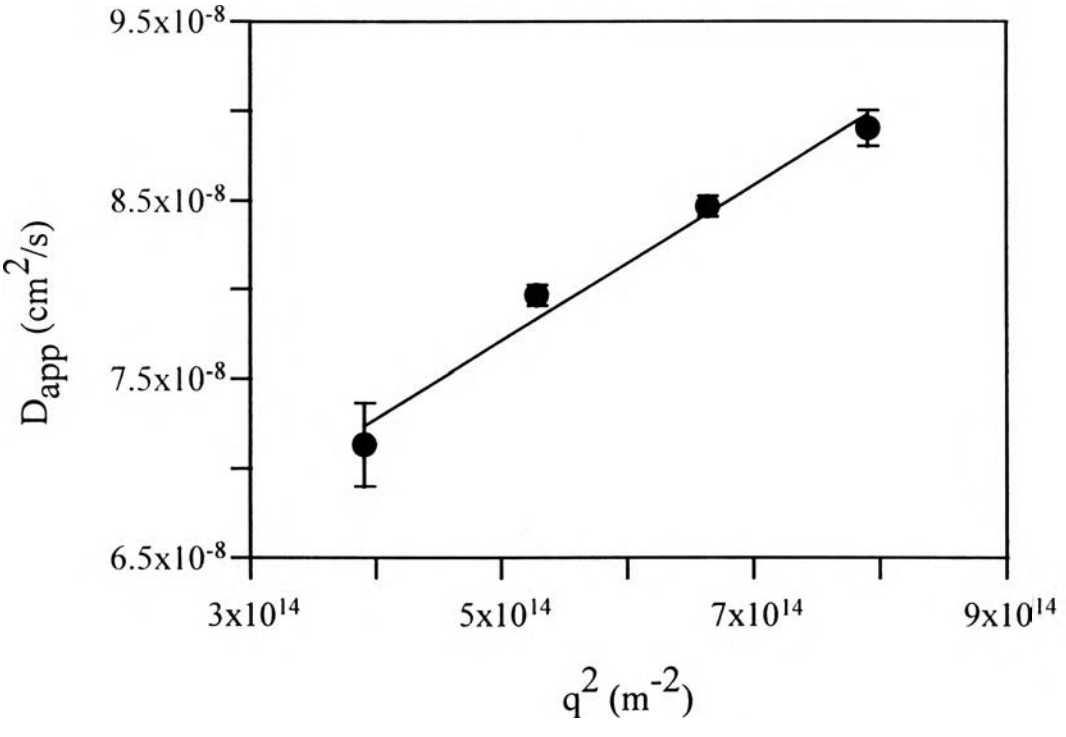

Figure 3.13 Apparent diffusion coefficient for complex system at the fixed C_{HPC} of 0.10%wt as a function of scattering wave vector square at 30°C.

Figure 3.14 shows D_{CM} and R_h of the complex system at fixed C_{HPC} of 0.06%wt and 0.10%wt versus surfactant concentration. We can divide C_{HTAB} into 4 regions, similar to the result of viscosity measurement. In Region I, no interaction occur so R_h is constant. At higher C_{HTAB}, Region II, R_h

decreases due to hydrophobic interactions of surfactant tails. After that R_h increases again because of electrostatic repulsion between surfactant head groups until reaching the maximum binding point. Both values of maximum binding points are nearly the same as these obtained from viscosity measurement. In Region IV, R_h decreases again due to screening effect from counterions.

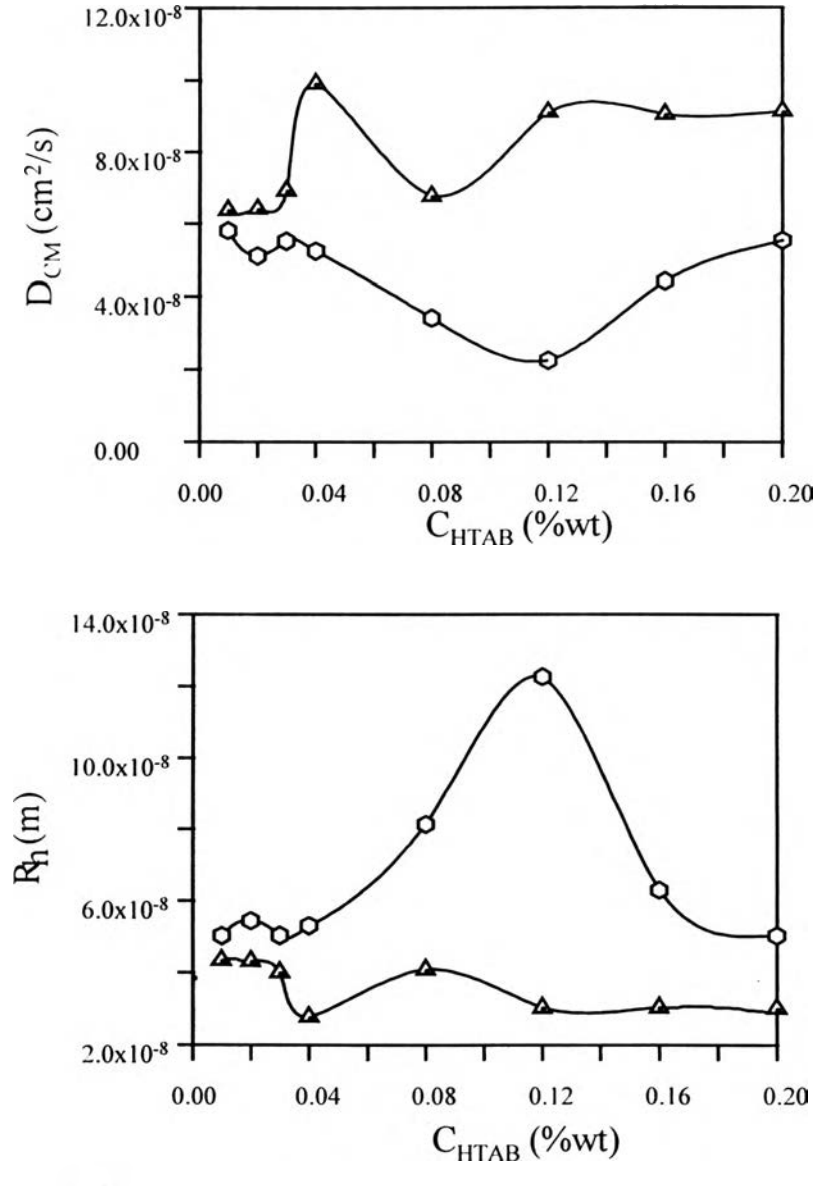

Figure 3.14 Diffusion coefficient and hydrodynamic radius of complex system as a function of surfactant concentration at 30°C : (Δ) C_{HPC} = 0.06%wt and (⬡) C_{HPC} = 0.10%wt.

Figure 3.15 shows polydispersity of relaxation time for complex solution at fixed C_{HPC} of 0.06%wt and 0.10%wt versus surfactant concentration at scattering wave vector of 90°. Polydispersity of relaxation time is $(\langle\Gamma'\rangle / \langle\Gamma\rangle)^2$ where $\langle\Gamma'\rangle$ is a standard deviation of characteristic decay time and $\langle\Gamma\rangle$ is a mean of characteristic decay time. Both plots increase and show the maximum value at C_{HTAB}=0.075. The range of polydispersity is from 0.50 to 0.95.

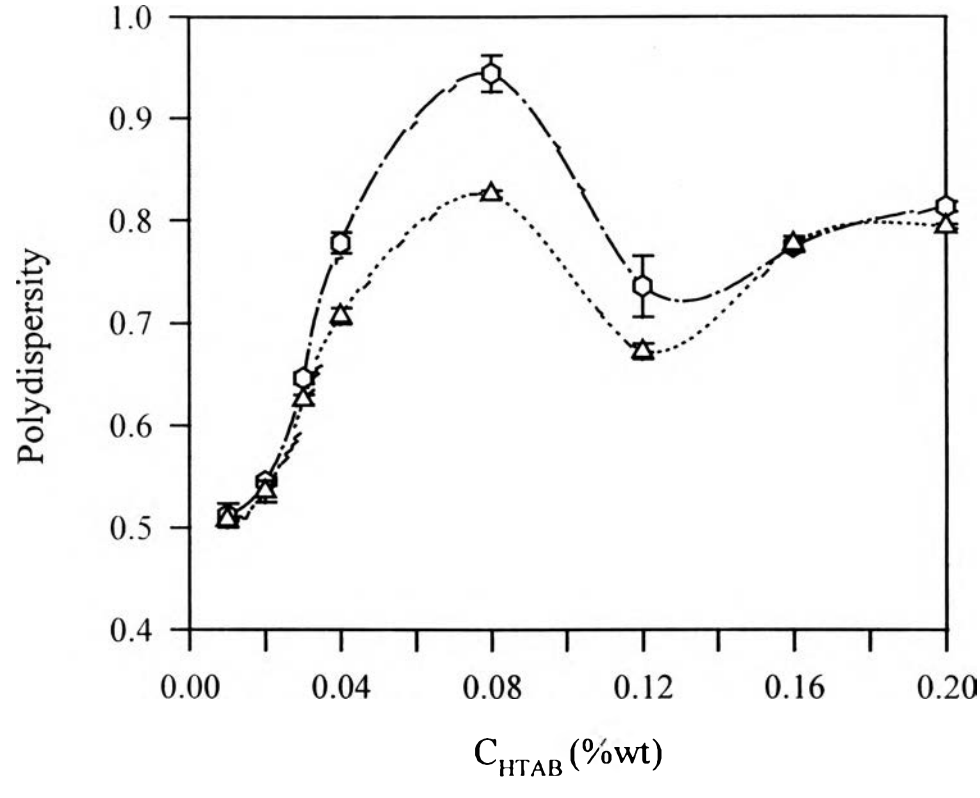

Figure 3.15 Polydispersity of relaxation time for complex solutions at 90° as a function of surfactant concentration at 30°C : (Δ) C_{HPC} = 0.06%wt and (○) C_{HPC} = 0.10%wt.

Table 3.2 Maximum binding points of complex at different polymer concentrations

C_{HPC}	C_{HTAB} at the maximum binding point		C_{HTAB}/C_{HPC}
	Viscosity	DLS	
0.02%wt	0.03%wt	-	1.500
0.04%wt	0.06%wt	-	1.500
0.06%wt	0.08%wt	0.080%wt	1.330
0.08%wt	0.09%wt	-	1.125
0.10%wt	0.13%wt	0.12%wt	1.250

From Table 3.2, the maximum binding points lie between 1.125 to 1.500. The average of all measurements is at $C_{HTAB}/C_{HPC} = 1.35$. This fixed value of C_{HTAB}/C_{HPC} was used in the sol-gel transition measurements which will be discussed later.

In Figure 3.16, the specific viscosities at fixed polymer concentration are shown versus the ratio of surfactant and polymer concentration, C_{HTAB}/C_{HPC}. We can see that in this plot the maximum points occur at nearly the same C_{HTAB}/C_{HPC} and that the shape of the plot of η_{sp} versus C_{HTAB}/C_{HPC} is nearly self-similar.

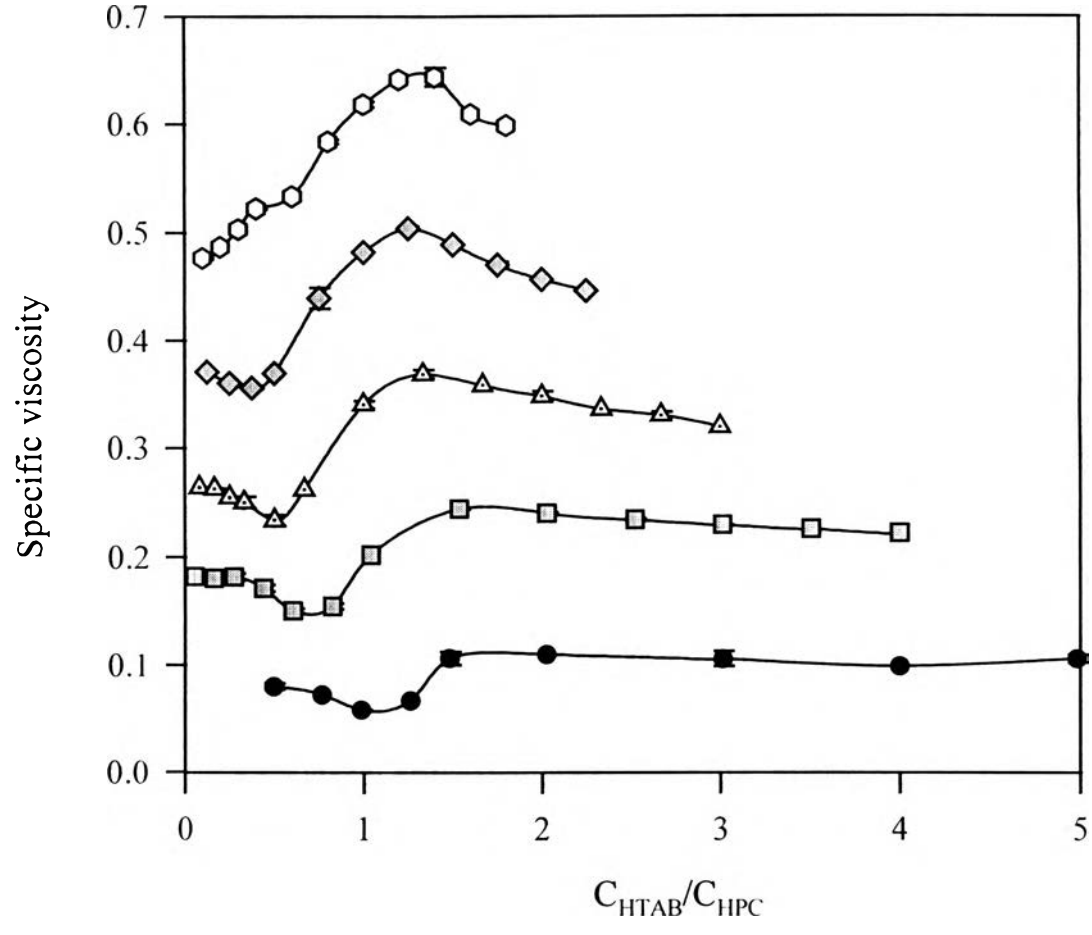

Figure 3.16 Specific viscosity of complex system at different polymer concentrations as a function of surfactant concentration at 30°C: (●) C_{HPC} =0.02%wt, (▣) C_{HPC} = 0.04%wt, (Δ) C_{HPC} = 0.06%wt, (◇) C_{HPC} = 0.08%wt and (⬡) C_{HPC} = 0.10%wt.

3.2 Concentrated Solution : Determination of Sol - Gel Transition

3.2.1 Binary System (HPC/Water)

The gel point (GP) of a thermoreversible gelling system may be determined by observing the frequency dependent loss tangent, tanδ, obtained from a multifrequency plot of tanδ versus temperature. Figures 3.17 a - c show tanδ versus temperature at various frequencies for HPC solutions at polymer concentrations equal to 3%wt, 4%wt and 5%wt. All systems exhibit a similar pattern of behavior, a steady decrease in tanδ with temperature, with the decrease being most significant for the lowest measurement frequency. The intersection of the curves, of different frequencies, is indicative of the GP; i.e. it identifies the particular temperature where the loss tangent first becomes frequency independent [Winter, 1991]. In Figures 3.17 a - c, the GP of all systems appear to occur at the same temperature, 48°C. Figures 3.18 shows plots of the loss tangent for the different polymer concentrations as a function of frequency at various temperatures. As expected, tanδ at GP is found to be practically independent of frequency for all systems. The results in Figures 3.18 confirm the location of the GP obtained from Figures 3.17.

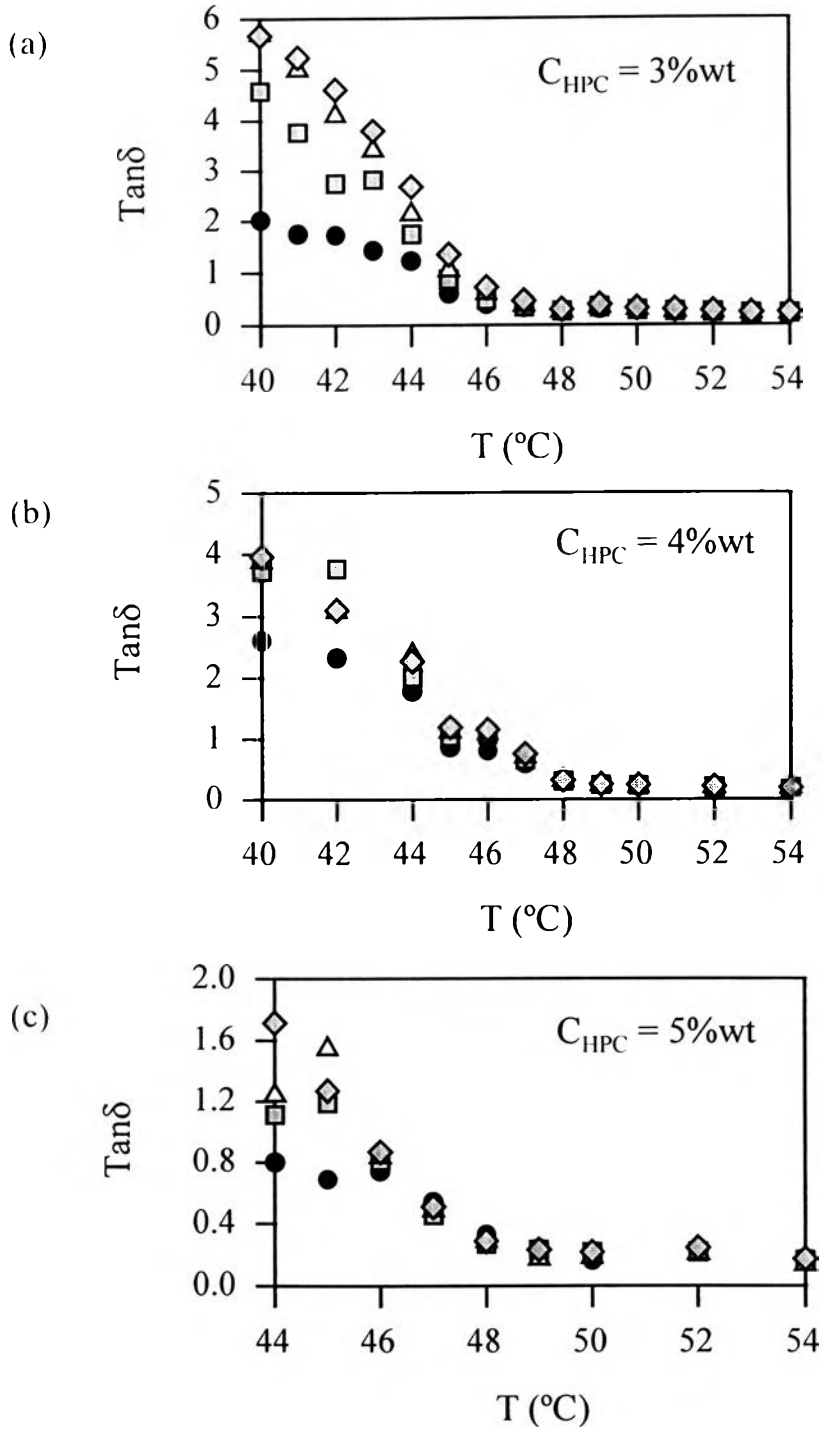

Figure 3.17 Viscoelastic loss tangent at different polymer concentrations : (a) C_{HPC} = 3%wt; (b) C_{HPC} = 4%wt and (c) C_{HPC} = 5%wt as a function of temperature at indicated frequencies: (●) ω = 0.2 rad/s; (□) ω = 0.5 rad/s; (△) ω = 1.0 rad/s and (◇) ω = 2.0 rad/s.

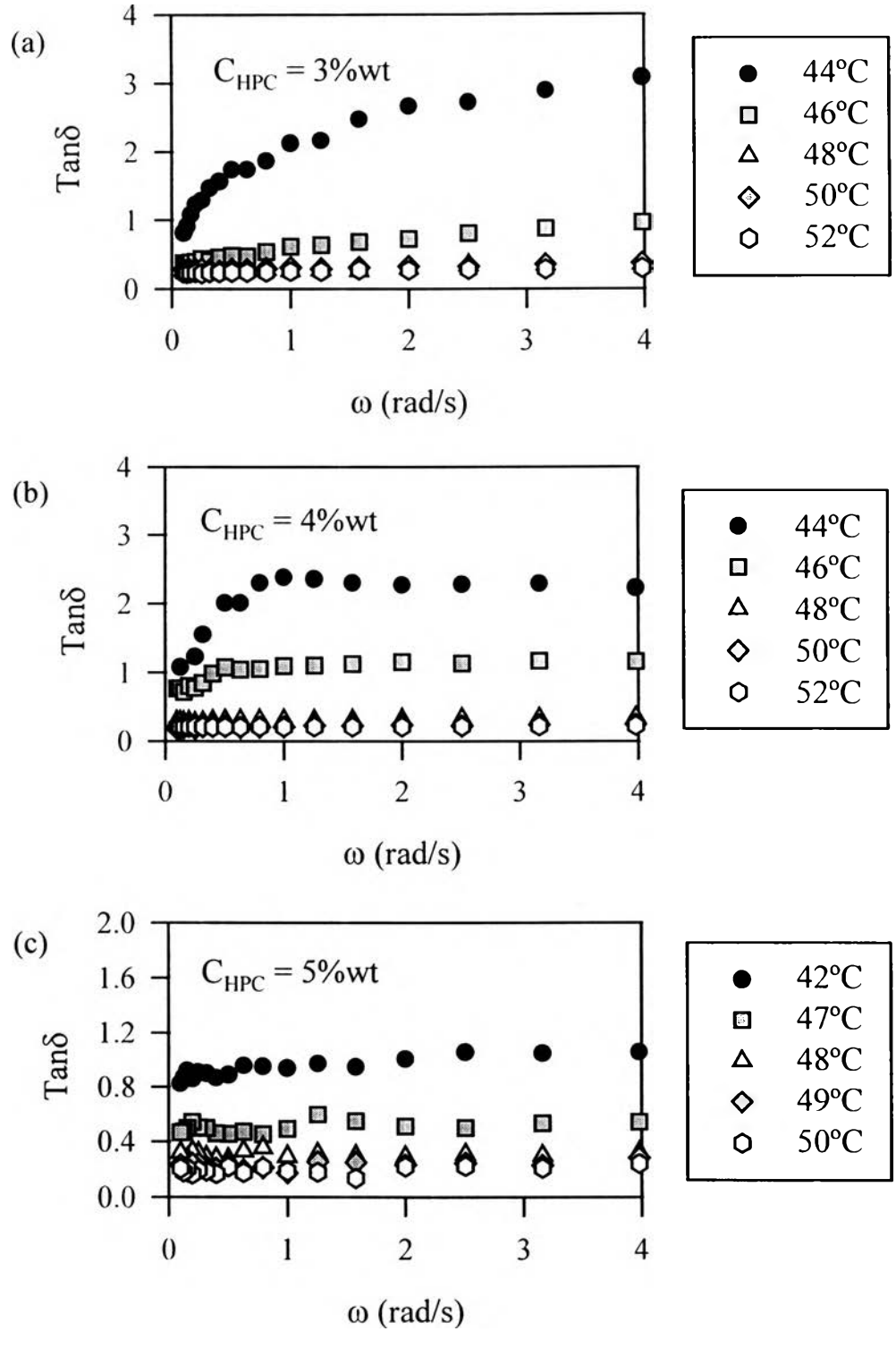

Figure 3.18 Frequency dependence of the loss tangent at different polymer concentrations at indicated temperatures: (a) C_{HPC} = 3%wt; (b) C_{HPC} = 4%wt and (c) C_{HPC} = 5%wt.

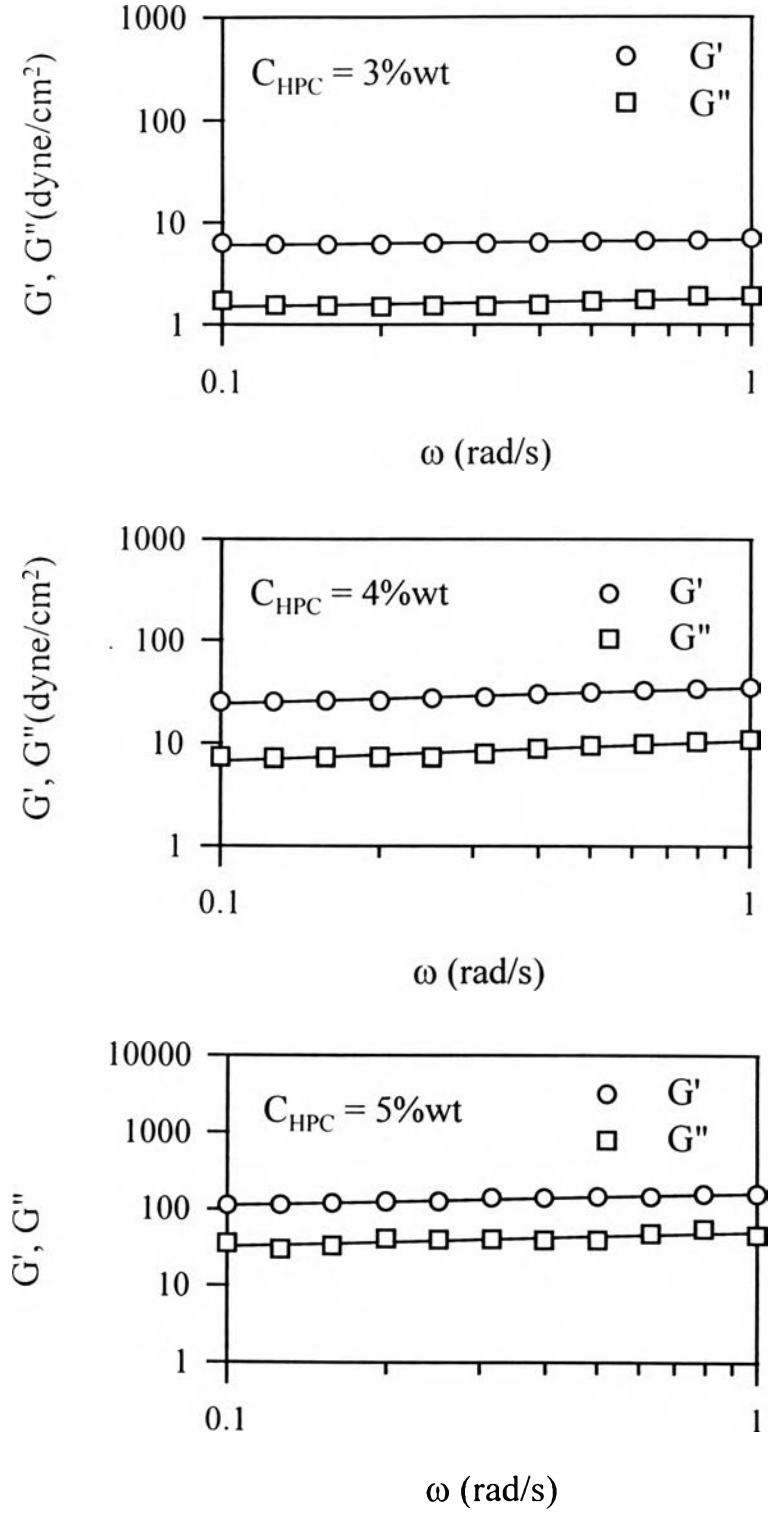

Figure 3.19 Plots of G′ and G″ vs frequencies for different polymer concentrations at the gel point showing the power law behavior: (a) C_{HPC} = 3%wt; (b) C_{HPC} = 4%wt and (c) C_{HPC} = 5%wt.

In Figures 3.19, the dynamic storage (G′) and loss modulus (G″) for different polymer concentrations were plotted against frequency at the GP (Equations 2.27 to 2.31). G′ and G″ of each system exhibit a power law behavior over a decade of frequency. The lines (least- square fits of the data to Equations 2.27 to 2.31) representing the power-law frequency dependence of G′ and G″ are essentially parallel and the resulting values of the scaling exponents n' and n'' are nearly equal. In these binary systems, at the gel points, G′ is substantially greater than G″ at each frequency. The results for the power-law fitting parameter for the binary system are summarized in Table 3.3.

Table 3.3 Power-law fitting parameters in binary systems at the sol-gel transition

Sample	GP	n	A	B	S (dyne/cm^2)
C_{HPC}=3%wt	48±1	0.06±0.01	6.76	1.79	0.19
C_{HPC}=4%wt	48±1	0.18±0.02	34.49	10.57	0.91
C_{HPC}=5%wt	48±1	0.19±0.02	161.77	49.97	4.27

Table 3.3 shows the concentration dependence of the viscoelastic exponent and the critical gel strength parameter for the binary systems at GP. The value of the power-law exponent increases with polymer concentration (from 0.06 to 0.19). Below, we will discuss the relationship of the exponent to the fractal dimension of polymer network structure. The gel strength parameter, S, which has been calculated from Equation 2.31, also increases with polymer concentration. A physical reason for S to increase with C_{HPC} is that a system with a greater chain density generally possesses a greater number of entanglement loci.

3.2.2 Ternary System (HPC/HTAB/Water)

For concentrated solutions of HPC/ HTAB complex, the ratio of surfactant and polymer concentration was fixed at 1.35, i.e. at the location of the binding saturation point. Table 3.4 shows the amounts of polymer and surfactant used in each sample solution.

Table 3.4 The amounts of polymer and surfactant in each sample solution

Sample number	Polymer concentration, C_{HPC}	Surfactant concentration, C_{HTAB}
1	3.0 %wt	4.05 %wt
2	4.0 %wt	5.40 %wt
3	4.5 %wt	6.08 %wt
4	5.0 %wt	6.75 %wt
5	5.5 %wt	7.43 %wt
6	6.0 %wt	8.10 %wt

Similar to the binary systems, the sol-gel transition can be defined as the temperature at which the loss tangent first becomes frequency independent. Figures 3.20a - c illustrate tanδ for complex systems versus temperature. The loss tangent becomes independent of frequency at 50°C, 49°C and 53°C for samples at fixed C_{HPC} = 4.0 %wt, 4.5 %wt and 5.0 %wt respectively.

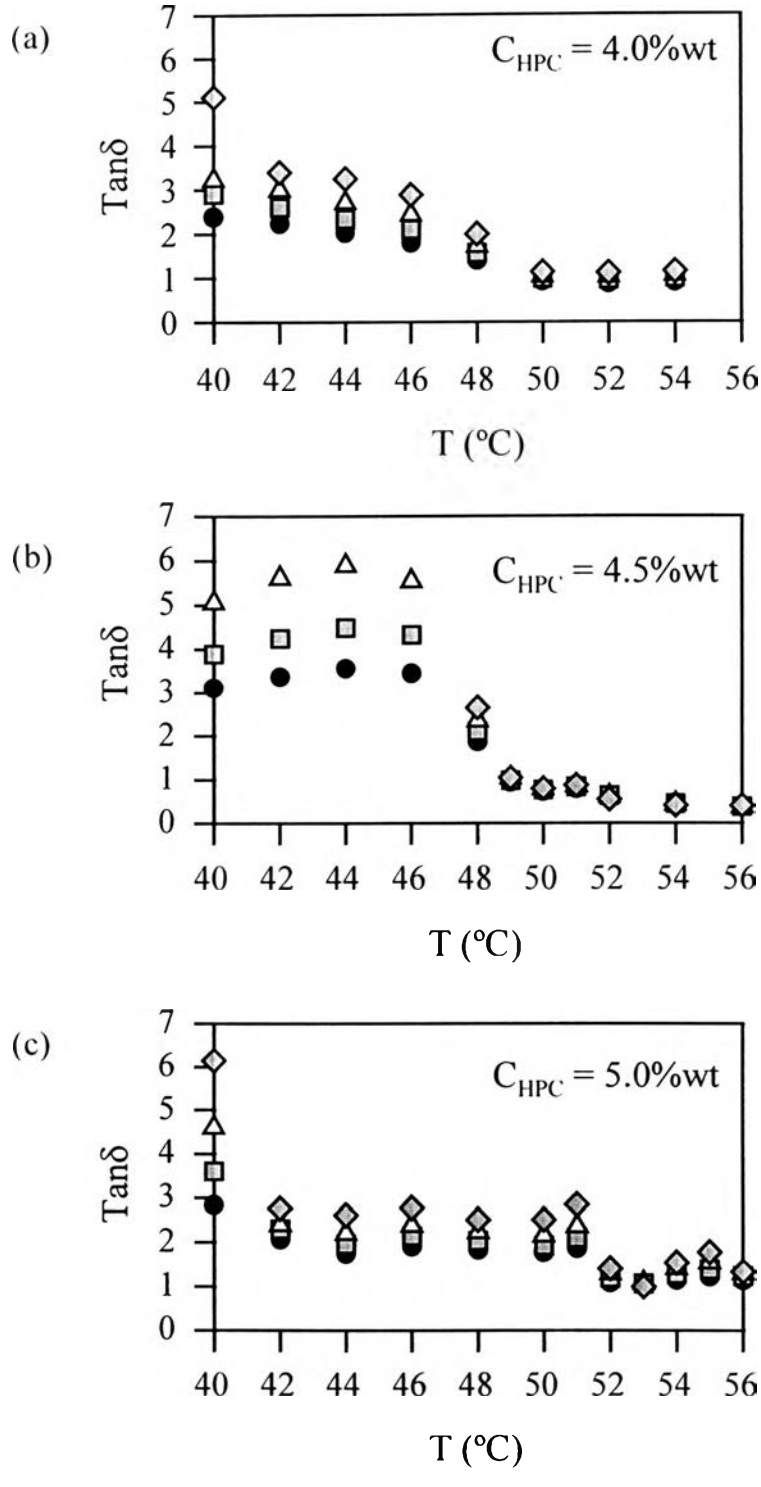

Figure 3.20 Viscoelastic loss tangent for complex systems: (a) C_{HPC} = 4.0%wt; (b) C_{HPC} = 4.5%wt and (c) C_{HPC} = 5.0%wt as a function of temperature at indicated frequencies: (●) ω = 0.2 rad/s; (□) ω = 0.5 rad/s; (Δ) ω = 1.0 rad/s and (◇) ω = 2.0 rad/s.

The gel points of the ternary systems appear shift to a slightly higher temperature with addition of surfactant. Figure 3.21 shows the plots of G′ and G″ for complex systems as a function of frequency at gel point. At the GP, G′ and G″ assume a linear dependence on frequency. Linear regression lines can be drawn through all data points. The lines are parallel and the power law feature is observed. The parameters from least square fits to Equations 2.27 to 2.31 for the complex systems are shown in Table 3.5. It should be observed that, for the ternary systems studied at the gel points, G′ is equal to G″ at all frequencies i.e. $\tan\delta = 1$. This result contrasts with that of the binary systems where $\tan\delta << 1.0$. Also, the value of the exponent n is much large ($n > 0.4$) than in the binary systems ($n < 0.10$)

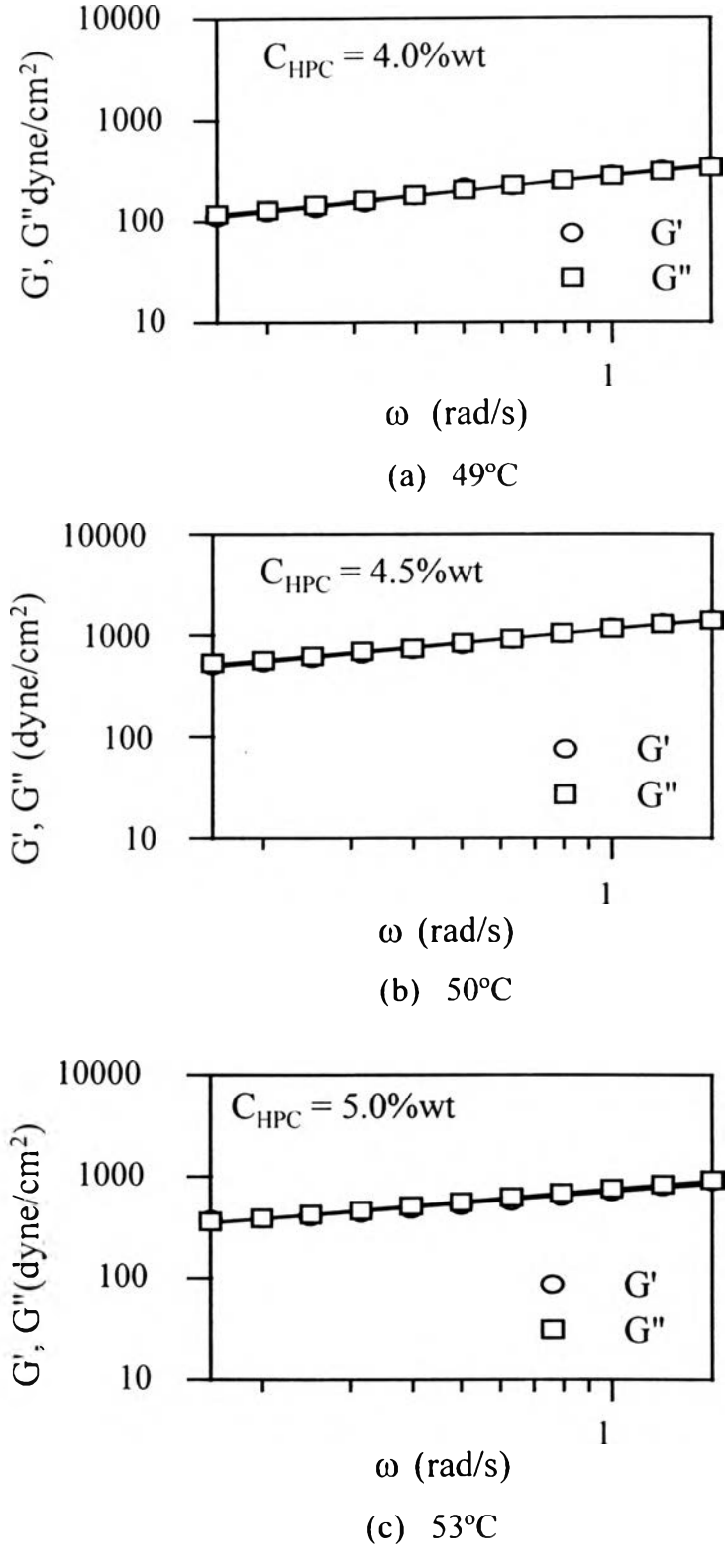

Figure 3.21 Plots of G′ and G″ vs frequencies at different polymer concentrations at the gel point showing the power law behavior: (a) C_{HPC} = 4.0%wt; (b) C_{HPC} = 4.5%wt and (c) C_{HPC} = 5.0%wt.

Table 3.5 Parameters of the ternary systems at sol-gel transition

Sample	GP	*n*	A	B	S (dyne/cm^2)
C_{HPC}=3.0%wt	-	-	-	-	-
C_{HPC}=4.0%wt	50±1	0.48±0.02	280	275	19.84
C_{HPC}=4.5%wt	49±1	0.45±0.01	1150	1140	39.32
C_{HPC}=5.0%wt	53±1	0.40±0.01	707	752	25.11
C_{HPC}=5.5%wt	-	-	-	-	-
C_{HPC}=6.0%wt	-	-	-	-	-

From Table 3.5, the concentration dependence of the viscoelastic exponent reveals some interesting features. The value of the power-law exponent of the complex system decreases slightly (from 0.48 to 0.40) with increase in polymer and surfactant concentrations. The critical gel strength parameter also appears to increase strongly with increase in polymer and surfactant concentrations.

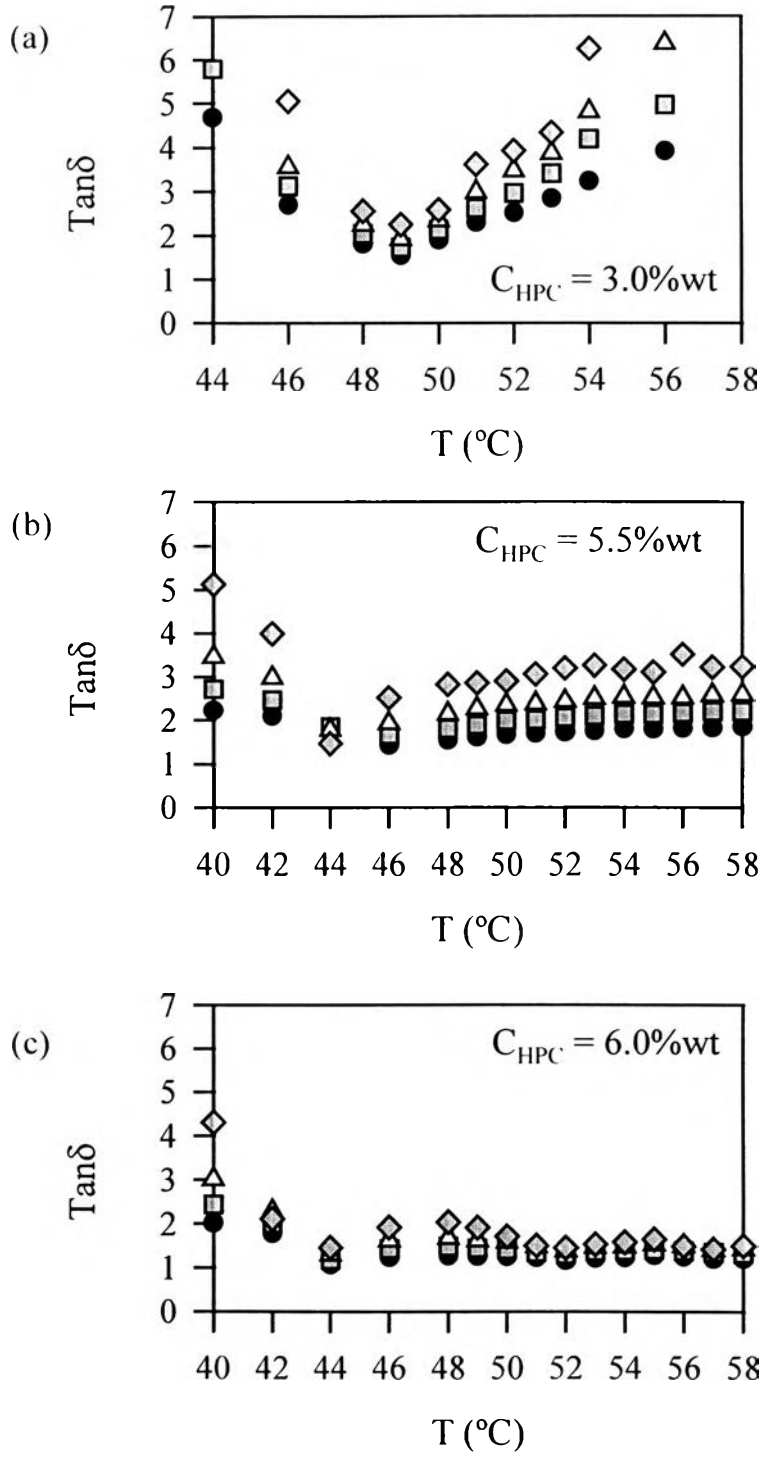

Figure 3.22 Viscoelastic loss tangent for complex systems: (a) C_{HPC} = 3.0%wt; (b) C_{HPC} = 5.5%wt and (c) C_{HPC} = 6.0%wt as a function of temperature at indicated frequencies : (●) ω = 0.2 rad/s, (▣) ω = 0.5 rad/s, (△) ω = 1.0 rad/s and (◇) ω = 2.0 rad/s.

In Figures 3.22 a - c, we show results of similar viscoelastic testing for the ternary mixtures containing HPC 3%wt, 5.5%wt and 6.0%wt, each at the HTAB/ HPC ratio equal to 1.35. No clear evidence of a physical gelation could be identified for these systems. This may indicate that the gelation follows a lower critical solution behavior with a critical concentration between 3%wt and 6%wt.

3.2.3 Mechanism and Gel Strength

For concentrated polymer solutions (HPC/Water system), polymer chains can overlap each other and form a transient network. An increase in temperature in the solution decreases the solvent quality and induces phase separation. The physical gelation of the HPC/ HTAB system reflects the huge elasticity of the concentrated HPC phase, which may exhibit liquid crystalline character. The GP occurs at 48°C and appears independent of polymer concentration. At this point, the gel strength increases with polymer concentration because, as the number of chains increases, it can be expected that the liquid crystal network will be strengthened.

For concentrated complex solutions (HPC/HTAB/Water system), the electrostatic interaction between bound micelles has to be taken into account. The bound micelles may induce gelation if they cross-link chains, or may retard gelation if the electrostatic repulsion prevent cross-links from forming. In the C_{HPC} 3%wt/HTAB/Water system, the number of chains appears to be not sufficient to cause formation of a physical gel. Therefore, a GP cannot be found in this system. For complex systems in which C_{HPC} = 4.0%wt, 4.5%wt and 5.0%wt, the GP temperature tends to increase relative to the binary solutions. The reason may be that the electrostatic repulsions of the complex polyelectrolyte chains tend to oppose network formation. More thermal energy must be added to overcome the electrostatic force. The gel strength at the gel

point increases because the formation of a polymer-surfactant complex in these systems resulting in chain expansion, i.e. a mono rigid chain. For the HPC/HTAB/Water system with C_{HPC} = 5.5%wt and 6.0%wt, the thermal energy cannot overcome the electrostatic repulsion between the polymer chains so a physical gel is not formed in these systems.

3.2.4 Fractal Dimension

Many theories have been proposed to relate the fractal dimension, d_f of the gel network to the viscoelastic properties of the gel. The fractal dimension is defined by $R^{df} \sim M$, where R is the radius of gyration of the gel cluster and M is the mass of the cluster. By considering the Rouse dynamics (hydrodynamic interaction is ignored), the effect of screening of the excluded-volume, and ignoring entanglement effects, the following expression for the power-law exponent, *n*, was derived for a monodisperse polymer system [Muthukumar, 1985]

$$n = d_f/(d_f + 2). \tag{3.4}$$

If corrections due to polydispersity effects of the clusters forming the incipient gel are taken into account, and Rouse dynamics prevails, the following relationship is obtained [Martin, 1989]

$$n = d_f(\tau - 1)/(d_f + 2), \tag{3.5}$$

where τ is the scaling exponent describing the cluster size distribution function near gel point. This polydispersity exponent is related to the fractal dimension ($\tau = 1 + d/d_f$), where d (d = 3) is the space dimension. By using percolation statistics ($d_f = 2.5$ and $\tau \cong 2.2$), *n* assumes a value of 2/3. The dynamic scaling

theory of Martin, which is based on the percolation theory and on the idea that the viscosity is dependent on cluster size, predicts a value of $n = 1$ in the Zimm limit (strong hydrodynamic interaction). The effect of polydispersity has been incorporated in the theoretical model of Muthukumar [1989]. It was assumed that variations in the strand length between cross-linking points of the incipient gel network give rise to changes in the excluded volume interaction. The surmise is that increasing strand length will enhance the screening of the excluded volume effect. When fully screened, the following expression emerges for a polydisperse system:

$$n = \frac{d(d + 2 - 2d_f)}{2(d + 2 - d_f)} . \tag{3.6}$$

All values of the scaling exponent for $0<n<1$ are possible for a fractal dimension value in the physically realizable domain $1<d_f<3$. In the case of unscreened excluded volume interaction the following relationship can be applied:

$$n = d/(d_f + 2). \tag{3.7}$$

In this case n changes from 1 to 3/5 as d_f varies from 1 to 3. From the rheological experiments, it is possible to estimate d_f using Equations (3.5) or (3.6). The results are shown in Table 3.6.

Table 3.6 Fractal dimensions for the binary and ternary systems

Systems	*n*	d_f from Martin, 1989	d_f from Muthukumar, 1989
HPC/Water			
C_{HPC}=3.0%wt	0.06	48.00	2.65
C_{HPC}=4.0%wt	0.18	14.67	2.34
C_{HPC}=5.0%wt	0.19	13.79	2.33
HPC/HTAB/Water			
C_{HPC}=4.0%wt	0.48	4.25	2.02
C_{HPC}=4.5%wt	0.45	4.67	2.06
C_{HPC}=5.0%wt	0.40	5.50	2.12

The different values of *n* and d_f determined between the binary and ternary system suggest that there is a difference in the gelation mechanism. There are some previous studies relative to gelation of polymer and polymer-surfactant complex systems. Lin *et al.* [1991] investigated crystallization induced gelation in the thermoplastic elastomer polypropylene and observed an exponent $n = 0.13$. The value of *n* was found to decrease slightly with the degree of crystallinity at the gel point. Scanlan and Winter [1991] studied end-linked poly(dimethylsiloxane) at GP, values of *n* are between 0.19 and 0.92, depending on stoichiometry, concentration, and polymer molecular weight. For the thermoreversible gelling system of gelatin, the values of the power law exponent are in the range 0.6 to 0.8 [Hsu and Jamieson, 1993]. Lindman *et al.*[1995] studied EHEC/CTAB and EHEC/SDS systems. They observed that *n* decreases slightly from 0.43 to 0.38 with EHEC concentration for the EHEC/CTAB system while for the EHEC/SDS system, an increase from 0.24 to 0.41 of *n* was detected.